FAR INFRARED LASER MAGNETIC RESONANCE

K. M. Evenson, R. J. Saykally[*], *and D. A. Jennings*

National Bureau of Standards
Boulder, Colorado

R. F. Curl, Jr.

Department of Chemistry
Rice University
Houston, Texas

and

J. M. Brown

Department of Chemistry
University of Southampton
Southampton, England

I. BASIC CONCEPTS

Within the last few years, laser magnetic resonance (LMR) has emerged as a powerful technique for the detection of transient species in the gas phase and the study of their rotational spectra. The sensitivity of this method is considerably higher than those of most competing techniques, such as conventional optical and microwave spectroscopy and gas-phase EPR, while the resolution attainable is comparable with that of the latter two methods. The domain of applicability of LMR presently includes atoms, ground states of molecules with up to 5 atoms, and most recently, short lived

---

[*] *Present address: Department of Chemistry*
University of California
Berkeley, California

ISBN 0-12-505405-X

metastable molecular electronic states, and molecular ions. The only rigorous constraint on this applicability is that the species of interest must be paramagnetic.

While LMR had its inception and early development in the far-infrared (FIR) region of the spectrum (40-900 μm), it has recently been extended to include vibrational transitions in the mid-IR (9-10 μm) and near-IR (5-6 μm), where it similarly has exhibited substantial capabilities. The laser Stark analogue of this technique has been developed quite effectively in the mid- and near-IR regions, although not yet in the far-infrared. In this paper we focus on the magnetic resonance methods in the far-IR. It is our hope to present a cogent and concise summary of the important features of laser magnetic resonance spectroscopy. First, we introduce the basic concepts of LMR, then the origin and development of the technique will be traced and salient results will be presented in Section II. In Section III, we describe the apparatus, and in Section IV, the dependence of sensitivity on the various experimental parameters will be elucidated. In Section V linear Zeeman theory will be used to assign a simple spectrum. Finally, the theoretical foundations for the analysis of LMR spectra are developed in Section VI.

LMR is intimately related to the technique of gas-phase electron paramagnetic resonance, (EPR),[1] so successfully exploited by Radford and by Carrington and his collaborators a decade ago. In both experiments appropriate paramagnetic energy levels of an absorbing sample are tuned by a DC magnetic field until their difference frequency equals that of a fixed-frequency source. The principal difference between these two experiments is that in EPR the relevant transition is between different magnetic sublevels (M_J) of the same angular momentum state (J), typically occurring in the microwave region for normally accessible laboratory magnetic fields (2 tesla); in LMR, the transitions are between rotational states in molecules or fine-structure levels in atoms, and the transitions occur in the far-infrared. In EPR, the transition can in principle be tuned to coincidence with any frequency lower than its maximum tunability (10 GHz, on the average), but in LMR one must rely on a near coincidence between the laser frequency and the transition frequency to within about 1%, given the same tunability. In each experiment the sample is contained inside a resonant cavity. The increased sensitivity of LMR is mainly derived from operating at frequencies roughly 100 times higher than those of the microwaves normally used in EPR, since absorption coefficients normally increase with either the square or the cube of frequency for $h\nu << kT$ and $\Delta\nu$(homogeneous) > $\Delta\nu$(Doppler). Also, by placing the absorbing sample inside the laser cavity,

additional sensitivity (up to 2 orders-of-magnitude) results from its interaction with the gain medium of the laser.

A schematic diagram of an LMR spectrometer is shown in Fig. 1. The laser oscillates between mirrors A and B in a

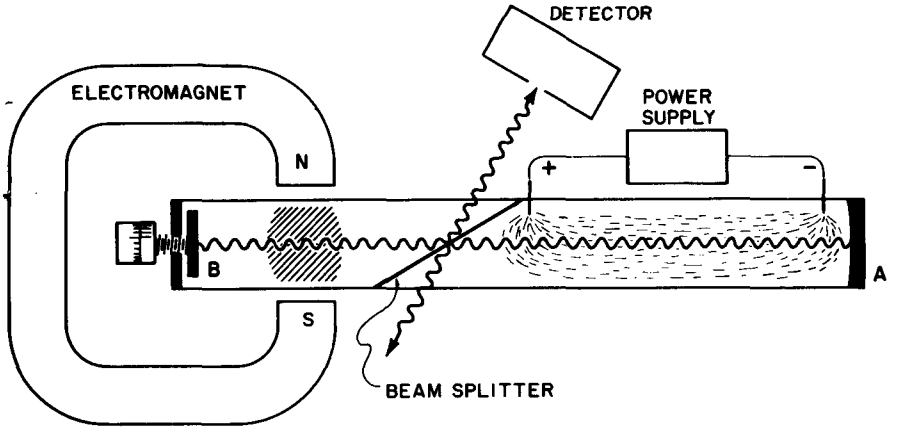

Fig. 1. Schematic diagram of far infrared electrical discharge laser magnetic resonance spectrometers.

single longitudinal mode. The cavity resonance can be tuned to the center of the gain curve by cavity length adjustment of mirror B. The polyethylene or polypropylene membrane window separates the intracavity sample cell on the left from the lasing medium on the right. Earlier designs incorporate discharge excitation in H_2O, D_2O etc. to generate cw lines in the 30 to 150 cm^{-1} range. Many more lines are now available by pumping CH_3OH, CH_3F and other gases with CO_2 laser radiation in place of the electric discharge. Indeed nearly 1000 cw lines from roughly 50 different gases have been made to oscillate in optically pumped FIR laser systems. These have been conveniently tabulated by Knight.[2] The frequency of many of these lines have been measured with a precision near 0.3 MHz (a few parts in 10^7). The intracavity absorption cell is located between the pole caps of a large electromagnet on which modulation coils have been wound. The cell is part of a flow system in which radicals are generated either directly in a 2450 MHz microwave discharge or by adding reactants to the products of a discharge close to the laser cavity. The beam splitter is set at the Brewster angle and polarizes the radiation. By rotation about the laser axis, transitions with either $\Delta M = 0$ or ± 1 can be selected. A small fraction of the radiation can be coupled by reflection from the beam

splitter to the detector, normally a helium cooled bolometer.

The detection limit for OH radicals by LMR is presently about 1 x 10^6 cm^{-3}, whereas for OH with EPR it is about 2 x 10^{10} cm^{-3}, for optical absorption it is about 10^{11} cm^{-3}, and for uv resonance fluorescence with a water vapor discharge source it is 3 x 10^9 cm^{-3}. The highest sensitivity for spectroscopic detection of OH radicals is obtained by laser induced fluorescence, 1 x 10^6 cm^{-3} in ambient air, but can be improved with optimum conditions.

The resolution in LMR can be either Doppler or pressure-broadening limited, depending on the conditions. Normal operating pressures are near 133 Pascal (1 Torr), which will produce a pressure broadened linewidth of ~10 MHz. The linewidth in Tesla also depends upon the magnetic tuning rate of the transition, which is typically ~10^4 MHz/Tesla, giving linewidths of ~10^{-3} Tesla. The Doppler width for a molecule with molecular weight of 25 at a frequency of 1 THz is 1.2 MHz, so that at normal operational pressures $\Delta\nu$(homogeneous) > $\Delta\nu$(Doppler). For suitably strong absorption signals, the pressure broadening can be reduced well below the Doppler width, and sub-Doppler saturated absorption (inverse Lamb dip) spectra can be obtained as a result of the intracavity operation of the spectrometer.

II. DEVELOPMENT AND CHRONOLOGY

Professor M. Mizushima first pointed out the near coincidence of the N, J = 5, 5 ← 3, 4 magnetic dipole transition of O_2 with the frequency of the HCN laser, and the possibility of Zeeman tuning these levels into coincidence with the laser. Subsequently, the first laser magnetic resonance signal was detected by Evenson, Broida, Wells, Mahler, and Mizushima[3] in 1968, in the study of this rotational Zeeman spectrum of O_2. The original spectrometer used the 337 μm line of an HCN discharge laser in conjunction with a Fabry-Perot resonator absorption cell located outside of the laser cavity. This external Fabry-Perot consisted of a 10 cm long cylinder, 1.7 cm in diameter with one flat mirror and one 15 cm focal length mirror. Each mirror had a 0.75 mm coupling hole so as to facilitate operation as a transmission cavity, whose Q was near 5 x 10^4. A Golay cell operating at 13.5 Hz was employed as the detector. Alignment and relative drift of the laser and the interferometer cavities constituted a serious experimental difficulty. Nevertheless, the N, J = 5, 5 ← 3, 4 magnetic dipole transition of the O_2 ground state was detected with a reasonable signal-to-noise ratio, as shown

on the right side of Fig. 2. The first derivative of the absorption is recorded because an ac magnetic field is superimposed on the dc field, and phase sensitive detection is employed.

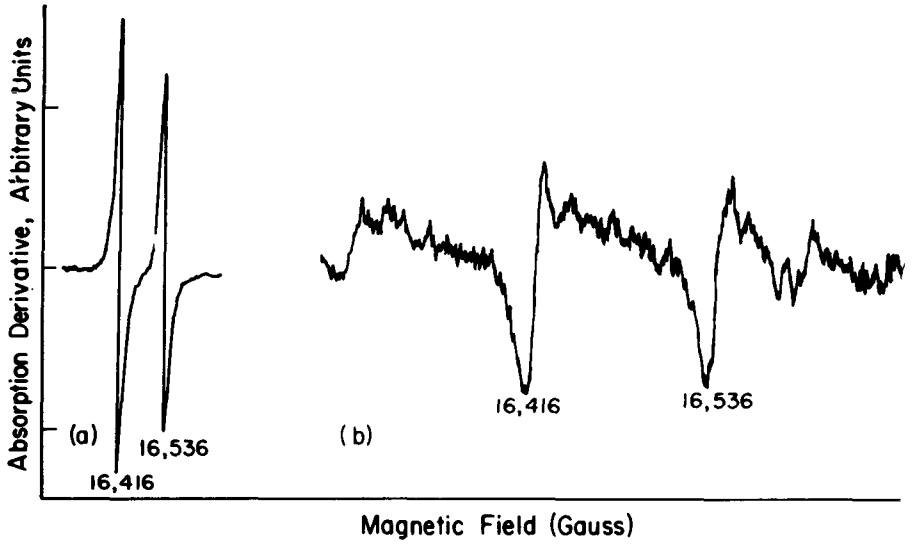

Fig. 2. (a) Trace of O_2 lines using intracavity 891 GHz LMB spectrometer using a 1 sec time constant. (b) Trace of same O_2 lines using external Fabry-Perot spectrometer and a 3 sec time constant. Both polarizations are present here.

Wells and Evenson[4] reported over an order-of-magnitude increase in the S/N ratio of this same O_2 transition sometime later, effected by making the absorption cell an integral part of the laser cavity. This increase was realized for several reasons: the effective path length (EPL) increased by a factor of 2 because of the higher finesse of the HCN laser cavity; power at the Golay cell was increased by a factor of 25, thus reducing the effects of detector noise; and, as we now know, interaction with the gain medium produced an amplification. A comparison between the S/N ratios from the intracavity and external cavity spectrometers is given in Fig. 2. This new spectrometer also incorporated the rotatable Brewster angle window dividing the laser discharge from the absorption cell, which produced the decided advantage of being able to select either σ or π polarization.

Laser magnetic resonance experiments using the HCN laser operating on the 337 - and 311 μm laser lines produced spectra

of both O_2[5] and NO_2.[6] In 1970, Evenson, Wells, and Radford[7] replaced the HCN laser with a water vapor laser, operating on the 78-, 79-, and 119 μm lines of H_2O, and used this system to observe the first LMR spectra of a transient molecule - OH. The 79.1 μm line was used to detect the $^2\Pi_{1/2}$, J = 1/2 ← $^2\Pi_{3/2}$, J = 3/2 transition, and the 118.6 μm line was used to observe J = 5/2 ← 3/2 in the $^2\Pi_{3/2}$ state. OH was formed by reacting atomic hydrogen, produced in a 2450 MHz discharge, with NO_2 in a flow tube.

Perhaps the single most important development of the LMR method occurred in 1971, when Evenson, Radford, and Moran[8] used the 118.6 μm H_2O laser line to detect the J = 7/2 ← 5/2, N = 3 ← 2 pure rotational transition of the extremely elusive CH radical in a low-pressure oxyacetylene flame. While EPR had yielded spectra of many similar transient radicals with $^2\Pi$ ground states, all attempts to observe such spectra from CH had failed. Similarly, astronomical searches for the 10 cm lambda-doubling transition had resulted only in frustration. The successful detection of CH clearly demonstrated the high sensitivity of the LMR technique; CH in the ground vibrational and rotational state yielded signals 260 times noise for an absorption path of 5 cm - roughly 30 times the S/N reported for an optical absorption experiment!

The observed LMR spectrum of CH is shown in Figure 3. Having achieved this high level of sensitivity, LMR studies of NO[9] and O_2[10,11] using the three H_2O laser lines, were published in 1972. In 1974, the detection of another important free radical - HO_2, the hydroperoxyl radical, of great significance in the upper atmosphere - was reported by Radford, Evenson, and Howard.[12] While poorly resolved electronic and vibrational spectra had been produced for HO_2 in earlier photolysis and matrix isolation studies, virtually nothing was known about its rotational spectra. LMR pure rotational transitions were observed in HO_2 with the three H_2O laser lines, and at 72-, 84-, and 108 μm with the D_2O laser. The analysis of these complicated LMR spectra without the availability of spectroscopic information from other sources, e.g., optical spectroscopy, presented a formidable challenge. Accordingly, Hougen[13] developed a general approach for assigning laser magnetic resonance molecular spectra without having prior knowledge of the molecular structure of the species responsible for them, and Hougen, Radford, Evenson, and Howard[14] analyzed the HO_2 LMR spectra in particular.

Even greater sensitivity had been effected with the water vapor laser system by replacing the ingenious but noisy Golay detector by a liquid helium cooled bolometer. The detection limit for OH was then determined to be 2×10^8 cm^{-3} - better than any spectroscopic technique existing at that time.

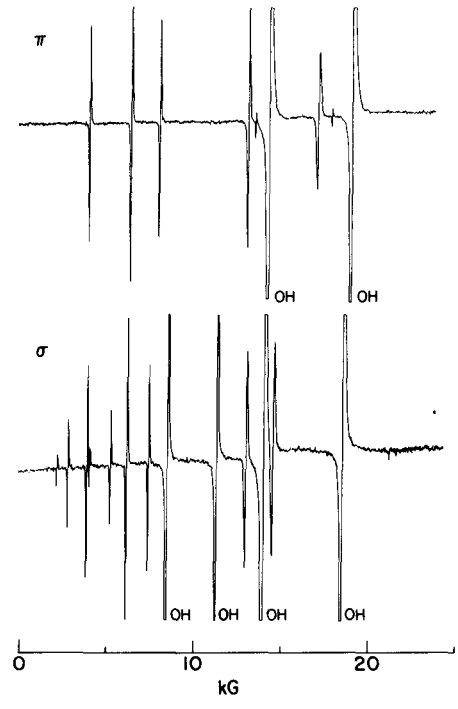

Fig. 3. The 118.6 μm H_2O laser magnetic resonance spectrum of CH produced by a low-pressure oxyacetylene flame.

Shortly after this work, Cook, Evenson, Howard, and Curl[15] reported the observation and analysis of the LMR spectrum of HCO, another nonlinear radical of considerable importance in flames. The $8_{2,6} \leftarrow 7_{1,7}$ transition was observed with the 108 μm D_2O laser line, with the HCO being generated by the reaction of atomic fluorine with formaldehyde.

Meanwhile, another group began to use an H_2O laser system for magnetic resonance spectroscopy; in 1975, Davies, Russell, Thrush, and Wayne[16] at Cambridge University reported detection of the amino radical (NH_2) by laser magnetic resonance. In their work, three different pure rotational transitions were observed at 78-, 118.6-, and 108 μm, and assigned to the $^2B_1$ ground state of NH_2. Shortly afterward, this same group reported the LMR spectrum of the PH[17] and PH_2[18] radicals, formed by reacting F atoms with phosphine (PH_3). The $6_{4,3} \leftarrow 5_{3,2}$ rotational transition of PH_2 ($^2B_1$) and N = 5 ← 4 transitions in the $X^3\Sigma^-$ and $a^1\Delta$ states of PH were detected with the 118.6 μm line of the H_2O laser.

By this point it had become clear that the high sensitivity, linearity, and versatility of LMR might make it a

powerful means by which the kinetics of certain very reactive intermediates could be studied. With a single water vapor oscillator, it would be possible to detect and measure quantitatively all of the free radicals HO_2, HCO, OH, CH, NH_2, PH_2, O_2, NO, and NO_2 at very low concentrations in mixed gas samples. Howard and Evenson[19] demonstrated that the peak-to-peak amplitude of the LMR signal was directly proportional to species concentration over large ranges if the total pressure and modulation amplitude were held constant during the run. (Surprisingly, the signal was largely independent of laser power).

Thus, by combining well-known flow reactor techniques with the laser magnetic resonance detection system, it became practical to study reactions involving unstable intermediates such as HCO and HO_2 by directly monitoring their concentrations. The chemistry of these two species in particular had remained uncertain for some time, precisely because such reactions had been studied only by indirect methods, in which the radicals themselves were not detected.

Howard and Evenson[19] tested the method on reactions of the hydroxyl radical (OH) with CO, NO, and NO_2. A diagram of the flow tube apparatus and the water vapor LMR detection system is shown in Fig. 4. In this work, OH was produced by the reaction of H atoms (from a 2450 MHz discharge) with NO_2 in the main flow tube. The OH radicals travel through the outer region of the flow tube along with a large excess of carrier gas (He or Ar). Reactant gas (e.g., CO) is added through the inner tube, which can be adjusted to a distance (z) from the detection volume. By monitoring the OH LMR signal and changing z, and thus the reaction time, a plot of ln [OH] vs z can be obtained. If the reactant gas (e.g. CO) is present in sufficient excess such that pseudo-first-order kinetics prevail, then this plot is linear, and $\frac{d\ln[OH]}{dt} = -k[CO]$. The time interval, dt, is given by $dt = \frac{dz}{\bar{v}}$, where $\bar{v}$ is the average flow velocity, in turn defined by $\bar{v} = \frac{1}{\pi r^2} \frac{760}{P_t} \frac{T}{273} F_t$, where r is the flow tube radius, P_t is the total pressure, T is the absolute temperature, and F_t is the total flow rate in standard cm^3/sec. Combining these expressions yields the relation $\bar{v} \frac{d\ln[OH]}{dz} = -k[CO]$; $\frac{d\ln[OH]}{dz}$ is the slope of the plot of ln[OH] vs z, and the CO concentration can be obtained by the relation $[CO] = \frac{F'_{CO}}{F_t} \times P_t \times \text{const}$, where the constant is simply the appropriate conversion factor. Therefore, the rate constant for the reaction $OH + CO \rightarrow CO_2 + H$ can be obtained directly.

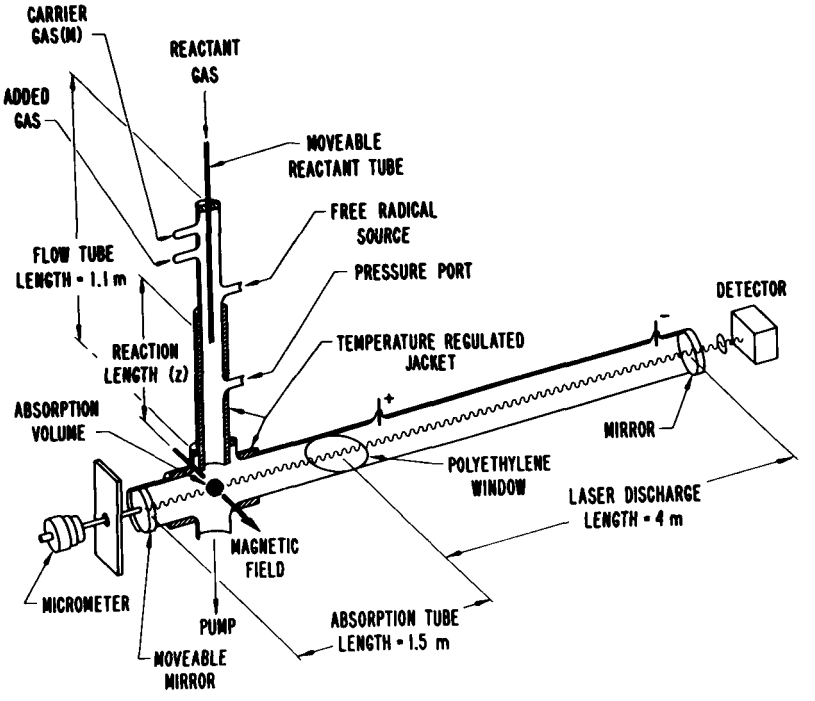

Fig. 4. Schematic diagram of LMR spectrometer with flow reactor used in kinetic studies.

Similar measurements were carried out for the reactants NO and NO_2. This work clearly established the potential of the LMR technique for kinetic studies of reactive intermediates.

Analogous studies of the reactions of OH with halogen-substituted methanes and ethanes were reported shortly afterward by Howard and Evenson,[20,21] and rate constants for OH reactions with ethylene and its halogenated derivatives were recently published by Howard.[22] These rate constants are of importance because of the role of halogenated hydrocarbons in conveying chlorine and bromine to the stratosphere, where the atomic species are photolyzed and released to catalytically destroy ozone. Reactions of OH with these halogenated hydrocarbons in the lower atmosphere compete with stratospheric photolysis as halocarbon sinks, and thus affect the ozone density.

The reaction $HO_2 + NO \rightarrow OH + NO_2$ is of importance in both photochemical smog and stratospheric chemistry. All previous kinetic data were based on indirect measurements, and as a consequence were quite imprecise. Howard and Evenson[23] measured the rate of this reaction using laser magnetic resonance

detection of HO_2, NO_2, and OH. This was a particularly interesting case, since all 4 species involved in the reaction can be monitored by LMR. The measured rate constant was 40 times faster than the previously accepted value. As discussed in a later paper by Crutzen and Howard,[24] the effect of this increased reaction rate was to increase the theoretical estimates of ozone depletions caused by continued use of industrial chlorocarbons while decreasing those expected from aircraft exhaust (which contains nitrogen oxides). In fact, an increased concentration of ozone due to stratospheric aviation is now predicated as a result of this increased value for the rate constant!

Howard[25] also measured the reaction rate of $HO_2 + NO_2$, and established the mechanism for this process. This reaction is also important to atmospheric chemistry. Thrush, Harris, and Burrows[26] have reported measurement of the rate constant for the reaction of HO_2 with OH and O, using the Cambridge water vapor laser system. Another group has also reported measurement of rate constants involving the HO_2 radical by the LMR method. Hack, Preuss, and Wagner,[27] of the Max Planck Institute in Göttingen studied the reactions $OH + HO_2 \rightarrow H_2O + O_2$, and Hack, Preuss, Wagner, and Hoyermann[28] studied the reaction of H with HO_2.

Recent studies made on the kinetics of reactions of atmospheric significance by LMR include measurement of the rate constant and temperature dependence of the $HO_2 + ClO$ reaction by Stimpfle, Perry, and Howard,[29] (a significant achievement, considering the difficulty of studying radical-radical reactions), measurement of temperature dependence of the rate constant for $HO_2 + NO$ by Howard,[30] and measurement of the rate constant for the very important reaction of HO_2 with O_3 by Zahniser and Howard.[31]

Clearly the use of laser magnetic resonance to monitor chemical reaction rates has had a marked impact on atmospheric chemistry, and on chemical kinetics in general. Presently, another group, led by Anderson and Radford (Harvard), is developing LMR systems to expand this application.

The scope of LMR was dramatically expanded as a result of the invention of the optically pumped far-infrared laser by Chang and Bridges[32] in 1970. The capabilities of LMR were quite evident from the experiments performed with H_2O and HCN lasers, but because the method relies on a close coincidence between a cw laser line and a relevant molecular transition, the general application of LMR as a spectroscopic technique seemed quite limited in scope: the total number of convenient laser lines from HCN and H_2O lasers is only 10! Furthermore, the wavelengths of all these lines were shorter than 337 μm (891 GHz), ostensibly limiting applications mainly to paramagnetic hydrides. With the advent and rapid development of

CO_2-pumped FIR lasers, the number of useful cw laser lines has grown rapidly to the present total of nearly 1000 - many of these in the wavelength region from 500 to 1000 μm. A histogram showing the number and distribution of these optically pumped cw FIR lines is given in Fig. 5. We now have very

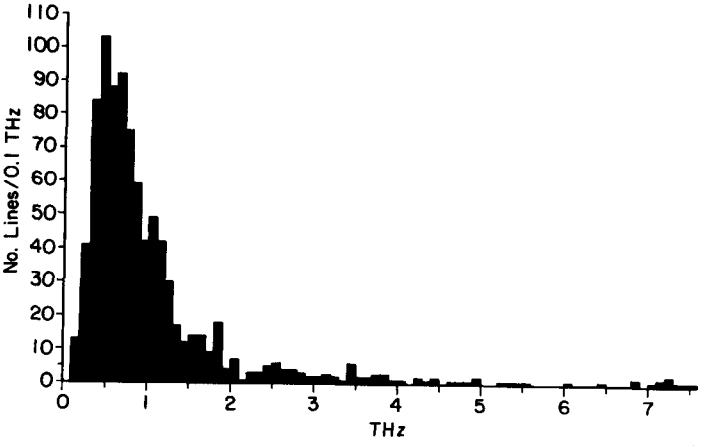

Fig. 5. Density of FIR optically pumped laser lines.

impressive coverage over most of the far-infrared region, and the power of laser magnetic resonance has grown accordingly.

The incorporation of the optically pumped laser design into a laser magnetic resonance spectrometer was achieved by Radford[33] in 1975. His system consisted of an optically pumped submillimeter gas laser 7.6 cm in diameter and 182.9 cm long, with one end being partitioned off with a Brewster window to form the intracavity absorption cell, located between the pole faces of a 30 cm magnet. The radiation from a 20 watt cw CO_2 laser was admitted to the FIR laser through a 2 mm hole in one end mirror to longitudinally pump the FIR lasing gas. This design presented an experimental difficulty, in that pump powers higher than 5 W would melt the polypropylene Brewster window. Attenuation of the pump laser power to avoid destruction of the window in turn limited the number of lines that would oscillate in this system to those with pumping thresholds below 5 W, about 30 lines at that time.

With this new design, Radford and Litvak[33] observed the imine (NH) radical LMR spectra from the $N = 1 \leftarrow 0$ transition with optically pumped laser lines at 302 μm (HCOOH) and 315 μm (CH_3NH_2). The NH radicals were generated by the reaction of F atoms with NH_3. Shortly afterward, Wayne and Radford[34] published an extensive analysis of LMR spectra of four imine isotopes. Radford also carried out additional measurements on the $NH_2(^2B_1)$ LMR spectrum, previously studied at Cambridge.[16] The twelve additional laser spectra he observed with the CO_2-

pumped system were combined with the earlier results from Davies et al.,[16] and analyzed by Davies, Russell, Thrush, and Radford[35] in 1978.

In 1977, Radford and Russell[36] observed another reactive molecule of substantial importance in flames and in atmospheric chemistry - the methoxy radical (CH_3O). This was the first definitive spectroscopic detection of CH_3O, which is extremely interesting from a spectroscopic point of view as well, since it exhibits several exotic effects characteristic of polyatomic molecules in degenerate electronic states, including large Zeeman and hyperfine anisotropies and possible Jahn-Teller distortion. Spectra possessing characteristic fourfold or twofold line splittings, resulting from a configuration with three identical spin 1/2 nuclei, were observed with optically pumped laser lines at 392, 394, 406, 419, and 513 μm. Methoxy was generated by reaction of F atoms with CH_3OH. A detailed analysis of these complex spectra is still underway.

In 1977, an improved design for an optically pumped LMR spectrometer with transverse pumping was developed by Evenson, et al.,[37] which will be described in Section III. This system has the advantage of accommodating higher CO_2 laser powers, and consequently operates on a larger number of FIR lines. Using this new system, Hougen et al.[38] observed new CH spectra with 8 optically pumped laser lines and obtained an improved signal-to-noise ratio, resulting from a more intense source of CH, viz. a F atom/CH_4 flame. They were able to make a rather complete analysis of six of the nine LMR spectra in this work, deducing values for the 4 hyperfine constants a, b, c, and d, as well as improved values for lambda doubling intervals in J = 3/2, 5/2, and 7/2 states.

A similar flame, F + CH_3F, yielded spectra that were identified as being due to CH_2F by Mucha et al.[39] The association of spectra detected on 4 laser lines with CH_2F was made on the basis of chemical and spectroscopic arguments. CH_2F was produced by reaction of F with CH_3F, or by the reaction of F atoms with CH_2N_2. The same spectra were later observed in a methane-F atom flame, although reduced by a factor of ten in intensity.

The Cambridge group also constructed an optically pumped LMR system of the Radford design. With this new spectrometer, Davies et al.[40] detected the $^3P_1$ - $^3P_0$ fine-structure transition in the ground state of oxygen atoms generated in a microwave discharge and flowed through the detection volume. They established the detection limit for O atoms by LMR to be 1-2 x 10^{12}. Most recently, Davies et al. have reported the detection and assignment of LMR spectra from SH(SD)[41] and SeH,[42] produced by flowing H(D) atoms formed in a discharge over solid sulfur or selenium, respectively.

The most recent results obtained by the Boulder group with the optically pumped LMR include detection of a series of radicals produced in methane-fluorine atom flames and measurement of the pure rotational spectrum of the metastable $a^1\Delta_g$ state of O_2.

Methylene radical (CH_2) was first observed in the LMR system by Mucha et al.,[43] who reported the detection of several hyperfine triplets. The identity of the carrier of these triplets was established as the $^3B_1$ ground state of CH_2 from a series of isotopic substitution experiments. Evenson, Saykally, and Hougen[44] have subsequently found several other sets of triplets, which have been shown to be from CH_2. A tentative assignment of the spectrum observed at 85.3 μm ($^{13}CH_3OH$) has yielded a structure for the radical, which, however, must be viewed as extremely tentative because of the obvious perils of using only one observed transition as the basis for such a determination. Another interesting result obtained in this study was the observation of a series of triplets at 171.8 μm ($^{13}CH_3OH$) occurring in stimulated emission.

The detection of the ethynyl radical (CCH) by LMR was reported by Saykally and Evenson[45] in 1978. The $N = 7 \leftarrow 6$ pure rotational transition in the $X^2\Sigma^+$ ground state was found using the 490 μm laser line of CD_3I. The identity of the carrier was again established through isotopic substitution experiments. This work constituted the first spectroscopic detection of gaseous CCH in the laboratory, although the observation of its microwave emission spectrum by radio astronomy has established it as a ubiquitous constituent of interstellar clouds.[46]

Observation and assignment of several spectra originating in the $X^2\Pi$ state of the CF radical has also been reported by Saykally and Evenson.[47] These spectra are among the most intense yet found with the optically pumped spectrometer.

The same authors[48] have also detected both the $2^3P_0 - 2^3P_1$ and $2^3P_1 - 2^3P_2$ fine-structure transitions within the carbon atom ground state in the same CH_4 + F flame that produced CCH, CH_2, CH, CH_2F, and CF spectra. The $J = 1 \leftarrow 0$ transition was measured with six different laser lines near 609 μm, while the $J = 2 \leftarrow 1$ was measured with 4 lines near 370 μm. Mass shifts and hyperfine splittings were observed for the ^{13}C isotope. Analysis of these measurements has yielded precise frequencies for the zero-field fine-structure transitions in both isotopic forms. The $J = 1 \leftarrow 0$ transition of ^{12}C has very recently been detected in several interstellar sources using these laboratory frequencies, as reported by Phillips et al.[77]

Pure rotational magnetic dipole spectra of the long-lived $a^1\Delta_g$ metastable excited electronic state of O_2 have been

observed in an afterglow of a 2450 MHz discharge through O_2 by Scalabrin, Mizushima, Saykally, Radford and Evenson.[49] Four different rotational transitions have been detected with four laser lines. The results are being combined with those of earlier EPR and optical spectroscopy experiments to obtain the best set of molecular constants for this state of O_2.

In 1978 Saykally and Evenson[50] reported the development of a new technique for studying transient species in a laser magnetic resonance system. In this system, the transverse iron core magnet has been replaced with a solenoidal magnet concentric with the laser axis, and the flame has been replaced by the positive column of a glow discharge plasma running along the magnetic field. The use of a live positive column plasma, instead of a flame or an afterglow, to produce transient species had quite recently resulted in the observation of three molecular ions (CO^+, HCO^+, HNN^+)[51-53] and several other very short-lived species[54-56] by microwave spectroscopy. The incorporation of this feature in a laser magnetic resonance spectrometer was intended to permit the observation of molecular ions by LMR as well.

This spectrometer has in fact produced several interesting new results. Saykally and Evenson have now reported the detection of oxygen atoms,[50] metastable excited electronic states of CO and O_2,[57] several ground-state radicals (OH, NH, HN_2), and the molecular ion HBr^+,[58] all generated in glow discharges through different gas mixtures.

The $2^3P_2 - 2^3P_1$ fine structure transition of atomic oxygen has been detected with the 63.1 μm laser line of $^{13}CH_3OH$ in a glow discharge through an O_2/He mixture. Three pure rotational transitions have been observed for the metastable $a^3\Pi$ state of carbon monoxide in discharge through 10% CO in helium. The average radiative lifetime of this state is 7.5 msec - very much shorter than the other metastables observed by LMR ($^1\Delta$ states of O_2 and PH). The $J = 9 \leftarrow 8$ transition of metastable $a^1\Delta_g$ O_2, also observed in the afterglow study discussed earlier, was detected in a discharge through pure O_2 with 392 μm laser line of HCOOH. The signal-to-noise ratio on this transition was sufficiently high to allow a large reduction of the O_2 pressure. A series of saturation dips were then observed, providing linewidths about ten times less than the Doppler widths.

The first laser magnetic resonance spectra of a molecular ion have been observed by Saykally and Evenson.[58] Four isotopic forms of HBr^+ ($H^{79}Br^+$, $D^{79}Br^+$, $H^{81}Br^+$, $D^{81}Br^+$) in its $^2\Pi_{3/2}$ ground state were detected in glow discharges through a dilute (1%) mixture of HBr (DBr) in helium. For the hydrogen isotopes, the $J = 5/2 \leftarrow 3/2$ transition was observed with laser lines at 251.1 μm (CH_3OH) and 253.7 μm (CD_3OH), the $J = 7/2 \leftarrow$

5/2 transition was detected with the 180.7 μm line of CD_3OH. The J = 7/2 ← 5/2 transition in v=1 was found with the 186.2 μm line of CH_3OH. The J = 5/2 ← 3/2 transition of DBr^+ was detected with the 496.1 μm line of CH_3F. All of the spectra showed hyperfine lines from both bromine isotopes and exhibited small lambda doublings. The proton hyperfine structure was not resolved. The 180.7 μm spectrum of HBr^+ is shown in Fig. 6. On a single Zeeman component of this transition, a

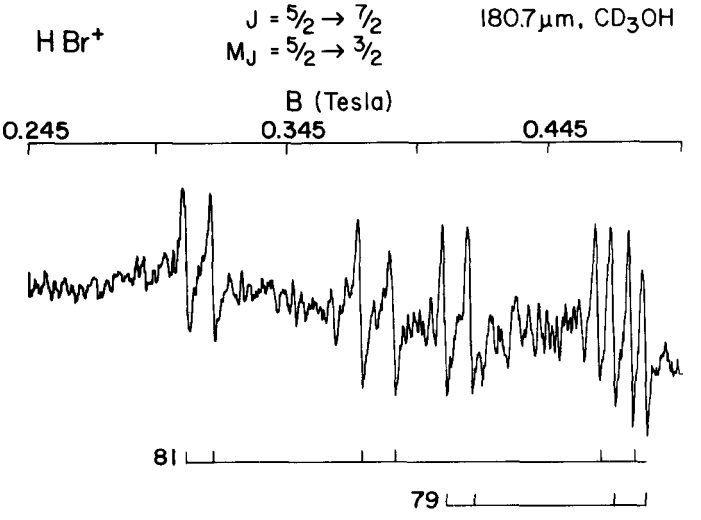

Fig. 6. LMR spectrum of HBr^+ taken with the 180.7 μm line of CD_3OH, $E_\omega \perp B_o$.

signal-to-noise ratio of ~100 was achieved with a 1 sec time constant on a single scan. In actuality this was quite a difficult experiment, because of the highly specific conditions required to produce the spectra; nevertheless, given a signal of this magnitude, other molecular ions should be detectable by the same method.

III. THE LMR SPECTROMETER

A schematic diagram of an optically pumped version of a laser magnetic resonance spectrometer is given in Fig. 7. This represents the current state-of-the-art in LMR spectrometer design; the earlier systems employing gas discharge lasers were similar in principle, and were shown in Fig. 1. In this optically pumped FIR LMR system, a suitable gas

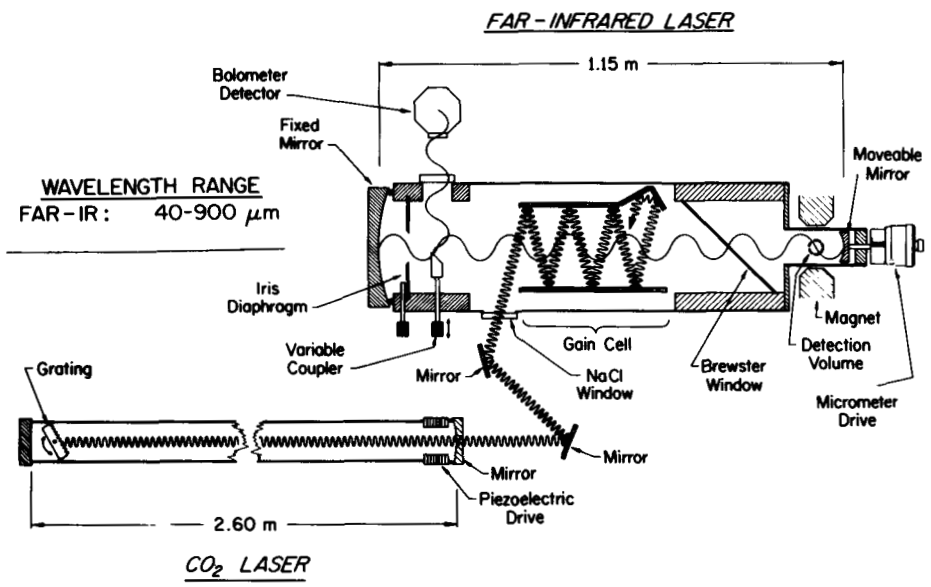

Fig. 7. Schematic diagram of an optically pumped far infrared LMR spectrometer.

(e.g. CH_3OH) having a strong vibrational absorption line coincident with a CO_2 laser frequency is pumped nearly transversely between parallel mirrors in the gain cell by a cw, grating and piezoelectrically tuned, CO_2 laser operating single mode with a power output near 50 W. The population inversion induced between rotational states in the excited vibrational state by the pumping action produces the far-infrared lasing action between appropriate rotational levels. The far-infrared radiation oscillates in the spectrometer cavity, defined by a fixed mirror at one end and a movable mirror attached to a micrometer drive at the other. The laser operates on a single frequency and is tunable over a narrow bandwidth. Single frequency operation occurs because the mode spacing $(\frac{c}{2\ell} \approx 150$ MHz) is much wider than the laser gain profile (~5 MHz). An iris is used to eliminate off-axis modes.

The gain cell of the laser, containing the optically pumped lasing gas, is separated from the sample region of the cavity by a 13 μm thick polypropylene window, set at the Brewster angle. This window serves several purposes. (i) it

provides the vacuum seal between the gain cell and the sample region of the cavity, (ii) it restricts the polarization of the laser to a single linear configuration, which can be oriented either parallel (π) or perpendicular (σ) to the magnetic field, and (iii) it can be used as a partial reflector to couple a fraction of the laser power out of the cavity onto a detector. The sample region of the laser cavity is positioned between the pole faces of a 38.1 cm (15") magnet with 15 cm pole tips operating with a 7.2 cm air gap. Fields slightly over 2.0 T can be produced in the 2 cm^3 detection volume defined by the intersection of the laser beam and the homogeneous magnetic field. A set of Helmholtz coils mounted on the pole faces provide a 1 kHz modulation field of up to $\sim 5 \times 10^{-3}$ T over the detection volume.

A liquid helium cooled germanium bolometer, operating with a NEP near 6×10^{-12} W $Hz^{-1/2}$ at 6.5 kHz is used as the detector. Typical powers absorbed by the radicals range from 0.3 to about 10^{-6} of the total laser power. A fraction of the laser power in the cavity is coupled out of the laser with a 45° copper mirror 4 mm in diameter on a small rod; the mirror is inserted a selected distance into the laser. The small fraction of the power reflected is directed through a polyethylene window located directly opposite the coupling mirror. With this scheme, the amount of power incident on the detector can be optimized for each individual laser line.

All of the species observed with this spectrometer are produced in various types of atomic and molecular flames reacting inside the detection volume pumped by a 10 ℓ/s mechanical pump. A concentric flow tube mounted on the laser system above the plane of the diagram and extending just down to the detection volume is the source of the flame.

In the LMR ion spectrometer, the positive column of a DC glow discharge is sustained in the sample region of the laser cavity, and the transverse magnetic field used in the previously described LMR experiments is replaced by a longitudinal field, provided by a 7.6 cm diameter and 33 cm long liquid nitrogen cooled solenoid magnet. This magnet is capable of producing a 5 kG field with a 0.1% homogeneity over a 15 cm length. The optically pumped gain cell is essentially the same as in Fig. 1. The longitudinal magnetic field configuration readily accommodates the live intracavity discharge, although producing some visible plasma constriction, and also provides an increased detection volume (~20 cm^3 instead of 2 cm^3). In operation it is essential to force the plasma down the center of the laser cavity by operating the cathode at a long distance from the solenoid.

IV. SENSITIVITY

In this section we consider the overall sensitivity of the LMR experiment and the adjustment of the experimental variables for maximum sensitivity. The analysis of sensitivity is broken into four parts as follows:

1. Discussion of the sources of noise combined with noise measurements to obtain the minimum detectable change in power at the detector due to that noise.
2. Measurement of the sensitivity of the LMR spectrometer in terms of a minimum absorption coefficient.
3. The limiting concentration for a typical molecule.
4. Comparison with other techniques.

Noise and Minimum Detectable Signal

The fundamental limitation on the minimum detectable signal which cannot be overcome by any improvement in detector or source is the quantum noise limit,[59] P_n. This minimum detectable power change at the detector is expressed by

$$\Delta P(\text{min}) = 4[PP_n]^{1/2}, \tag{1}$$

where,

$$P_n = h\nu B/[1-\exp(-h\nu/kT)], \text{ and} \tag{2}$$

P is the total power on the detector, P_n is the laser noise, and B is the bandwidth of the detector. For the typical LMR experiment with ν = 1.5 THz, T = 300 K, and a bandwidth, B, of 1 Hz, P_n is 4.7 x 10^{-21} W. In LMR, a typical value of the power reaching the detector is 2.5 x 10^{-5} W which results in a value of 1.4 x 10^{-12} W for $\Delta P(\text{min})$.

The quantum noise limit is never achieved in practice. Usually the limiting noise is either detector noise or source noise. For the Ge bolometer detector viewing the non-oscillating FIR laser, the NEP is about 6 x 10^{-12} W for a 1 Hz bandwidth, so that detector noise is only a factor of 4 greater than the quantum noise limit. Source (or local oscillator) noise arises from various physical fluctuations which result in laser amplitude instability such as vibrations, ripple, power line fluctuations and plasma noise which may be present in either the FIR laser or the CO_2 pump laser. Because of the variety of origins for source noise, it must be estimated by experimental measurement. It is found experimentally that the

amount of source noise observed depends on the IF (i.e., modulation) frequency and decreases with increasing IF frequency. The frequency response of the bolometer detector (half-power points at 1 kHz) sets a maximum IF of about 6.5 kHz before the loss in signal overcomes the reduction in source noise. At the optimum IF frequency of about 6.5 kHz, the noise at the phase sensitive detector output decreases by about one half when the FIR beam is blocked on the stronger lasing lines. Thus with the present lasers the minimum detectable change in power at the detector is limited by laser amplitude fluctuations (source noise) and is about 10^{-11} W for the stronger laser lines but is less than the detector noise for the weaker lines.

With improvement in both the stability of the laser and in the noise level of the detector a factor of 7 might be gained in overall sensitivity; however, since the noise level of each is similar, both would have to be improved to effect the increase in sensitivity. We are quite close to the quantum limit!

Measured Sensitivity

Before reporting experimental measurements of the LMR spectrometer sensitivity it seems worthwhile to briefly review some elementary relationships which affect the signal size (see Reference 59 and references therein).

The power reaching the detector, P_{out}, is coupled out of the FIR laser cavity

$$P_{out} = CP_{in}, \tag{3}$$

where C is the output coupling and P_{in} is the level of the circulating power inside the laser. Thus the change in power at the detector on introduction of the molecular absorption is proportional to the change in the level of circulating power inside the laser. The operating point of any oscillator is determined by the condition that the gain (which is a function of the level of oscillation) equals the loss (which normally is independent of the level of oscillation).

$$G(P_{in}) = L \tag{4}$$

Thus on introducing a small additional loss, we have

$$\Delta P_{in} = \Delta L \frac{dP}{dG} \text{ or } \frac{\Delta P_{out}}{\Delta L} = C\frac{dP}{dG}. \tag{5}$$

An adequate model of the FIR laser would be required in order to calculate dP/dG. Several attempts were made in an effort to develop a model which explains the measured experimental parameters of the LMR spectrometer. Our efforts have not been successful. In lieu of theoretical expressions we offer instead, experimentally observed operating conditions and empirical relationships.

The instrumental sensitivity, $\frac{\Delta P_{out}}{\Delta L}$, (i.e., the change in output power when a small additional loss, ΔL, is introduced into the laser cavity) was directly measured by rotating a specially constructed beam splitter inside the laser cavity. The reflectivity of the 12.5 μm thick beam splitter for a 2° change was measured outside the cavity and agreed with the value calculated from the measured polypropylene index of refraction at 118.8 μm (n = 1.522). By measuring the laser output power, then rotating the beam splitter to introduce a known small additional reflection loss, the sensitivity was measured experimentally, and the minimum detectable one way loss, $\Delta L_{min} = (\frac{\Delta L}{\Delta P_{out}}) P_{noise}$, was determined for both the 163.0 and 118.8 μm CH_3OH laser lines. First, however, the sensitivity was optimized by observing the S/N ratio for O_2 LMR lines by varying the laser coupling, CO_2 laser pump power, methanol pressure, and foreign gas (He) pressure (in the gain cell). It was found that the best S/N was obtained with the maximum foreign gas pressure consistent with stable laser operation and with the maximum CO_2 laser power available. In increasing both the foreign gas pressure and the CO_2 laser power, the S/N ratio levels off after an initial rapid increase so that it is not a sensitive function of these parameters near the optimum operating conditions. The S/N of the O_2 lines was also studied as a function of the output coupling, and was largest for the maximum coupling obtainable (overcoupled with respect to maximum power) with the small coupling mirror employed. Again the S/N was not found to be a particularly sensitive function of the output coupling once the laser noise became the dominating noise, for each increased as the coupling was increased. After optimizing the signal with each laser line, identical sensitivities of $\Delta L_{min} = 2 \times 10^{-10}$ were obtained.

The empirical behavior of the LMR spectrometer can be summarized by the equation

$$\Delta P \propto \frac{C \Delta L_P}{L} , \tag{6}$$

where ΔP is the LMR signal, measured as a change in power at the detector (not a fractional change), C is the coupling

parameter, ΔL is the loss due to the paramagnetic sample, p is the foreign gas pressure (He) in the gain cell, and L is the total round trip loss of the FIR resonator. In general, one can say:

1. The coupling, C, should make the laser over coupled, but not so much as to make it unstable,
2. the foreign gas pressure should be high,(100-300 Pascals) but again as in 1, not to decrease the laser power to the point of instability, and
3. the overall loss, L, should be as low as possible (usually it is about 2 to 4%).

We have also found that well above threshold the signal, ΔP, is nearly independent of the FIR power. This result is in agreement with earlier measurements made with the H_2O discharge LMR spectrometer.

The measurements and calculations described above provide one with some insights into the physical basis of the LMR experiment; however, another estimate of the sensitivity of LMR is provided from measurement of S/N ratios of absorption lines. O_2 is a convenient reference substance in that it is paramagnetic, stable, and the weakly allowed magnetic dipole transitions are not susceptible to laser power saturation at the laser powers normally used. Therefore, the S/N ratios were measured for three weak O_2 lines using the methanol laser lines at 118.8, 163.0 and 699.5 μm. The lines chosen were the lowest field lines with perpendicular polarization (i.e., the magnetic field of the laser is perpendicular to the Zeeman field) and are the weakest observed at each wavelength. The results of these measurements are given in Table 1 along with the magnetic fields of these calibration lines. These lines may be useful for sensitivity comparisons with other spectrometers.

If similar measurements of sensitivity were made in an external cell, ΔL_{min} would be simply the fractional laser noise: 4×10^{-7} at one Hz. The increase in sensitivity by using intracavity absorption is obtained by dividing this number by ΔL_{min} for the cavity. The increase is thus 1000; a very significant improvement is obtained with the intracavity technique. The actual path length is determined by the length across the homogeneous magnetic field (about 1.5 cm); the effective path length is about 1500 cm. If an external passive Fabry-Perot cavity were used, ℓ(eff) would be $\ell(F/\pi)$ where F, the finesse, is $\frac{\pi\sqrt{R}}{(1-R)}$ and R = reflectivity of mirror ($\simeq$0.98). Thus, ℓ_{eff} is given by:

$$\ell_{eff} = \frac{2\ell}{\text{Round trip loss}} . \qquad (7)$$

TABLE 1. Comparison of Minimum Detectable Loss Obtained From Beam Splitter Measurements with that Obtained from O_2 Absorption

	O_2 Measurement (1 Torr)				Beam Splitter
λ (μm)	Magnetic Field (10^{-4}T) [a]	S/N [c]	γ_o (cm^{-1}) [d]	ΔL_{min} [e]	ΔL_{min}
118.8	3.933 [b]	500	1.2×10^{-7}	4×10^{-10}	2×10^{-10}
163.0	5.254	700	3.7×10^{-7}	8×10^{-10}	2×10^{-10}
699.5	1.094	3160	40×10^{-7}	20×10^{-10}	——

[a] $B_\omega \perp B_o$

[b] This same transition is observable on the 118.6 μm line of H_2O @ 4.935×10^{-4}T.

[c] One second time constant.

[d] γ_o is the absorption coefficient calculated from Eq. 7c in reference 10.

[e] L is one way absorption: $\Delta L = \gamma_o(\ell)$. ($\ell \approx 1.5$ cm, here).

The round trip loss in the laser cavity is about 4%: and ℓ_{eff} would be 75 cm. It appears that the presence of the gain medium produces an enhancement of sensitivity by a factor of 20.

Relationship of Intracavity Loss to Molecular Concentration

In order to estimate the spectroscopic sensitivity of LMR, it is now necessary to relate the minimum detectable loss ($\Delta L_{min} \approx 4 \times 10^{-10}$) to the properties and concentration of molecules. This task could be greatly complicated by power saturation effects which must be introduced in the integration over the sample volume. Fortunately the normal sample pressures (1 Torr) and intracavity intensities (<10 mW/cm^2) are such that power saturation of the sample absorption is negligible when the laser power is decreased by the addition of helium in the gain cell. This both increases the sensitivity

and prevents saturation of the detector (about 25 μW is the optimum power). Lamb dips can be seen with this LMR apparatus but only when the pressure is reduced approximately tenfold. This tenfold reduction corresponds to a hundredfold increase in saturation.

In the absence of power saturation, the change in the cavity losses on introducing the molecular absorption for π transitions (ΔM = 0) is given by

$$\Delta L = \nu S^{\alpha}_{J,\tau,J',\tau'} |\mu_{\alpha}|^2 \, n_{J,\tau,M} \frac{(1-\exp(-h\nu/kT))}{(c\hbar\varepsilon_o\Delta)} (\ell) \left| \begin{pmatrix} J & 1 & J' \\ -M & 0 & M \end{pmatrix} \right|^2 , \tag{8}$$

where $S^{\alpha}_{J,\tau,J',\tau}$ is the line strength for a rotational transition allowed by molecular dipole component, μ_{α}, $n_{J,\tau,M}$ is the number of molecules/unit volume in the lower state (J,τ,M) of the transition, Δ is the HWHM of the line (here assumed Lorentzian), and the path length in the sample is ℓ. The number density of molecules in the lower state of the transition is related to the total number of molecules/unit volume by

$$n_{J,\tau,M} = N\exp(-E_{J,\tau,M}/kT)/Q . \tag{9}$$

where Q is the internal partition function. Introducing Eq. (9) into Eq. (8), the result is

$$\Delta L = \nu S^{\alpha}_{J,\tau,J',\tau'} |\mu_{\alpha}|^2 \frac{N\exp(E_{J,\tau,M}/kT)(1-\exp(-h\nu/kT))}{(c\hbar\varepsilon_o\Delta Q)} (\ell) \left| \begin{pmatrix} J & 1 & J' \\ -M & 0 & M \end{pmatrix} \right|^2 . \tag{10}$$

From the previous sections we have seen that the minimum detectable ΔL is approximately 4×10^{-10}. Let us estimate the minimum detectable number density of molecules, N, in a typical case. The pathlength, ℓ, over which the magnetic field is homogeneous is about 1.5 cm. For a polar molecule the permanent dipole moment component, μ_{α}, is typically 1 Debye, a typical line strength $(3J)^2$ product is 0.5; a typical linewidth, Δ, at 1 Torr is 10 MHz. For a light molecule, Q, the partition function, is of the order of 200. $E_{J,\tau,M}$ might be about kT, with T = 300 K. Upon introducing these numbers, the minimum detectable number of molecules/unit volume becomes $5 \times 10^7/cm^3$ for a transition at 1.5 THz. A sensitivity of 10^6 cm^{-3} for OH has been measured in the water vapor spectrometer; this is in agreement with the above number since OH has a 3

times greater dipole moment and a smaller Q. Also, a somewhat longer path was provided by a more homogeneous magnet and the sensitivity of the water vapor laser may be somewhat different.

Comparison of Sensitivity of FIR LMR with that of Other Techniques

We now wish to compare the sensitivity of LMR in the far-infrared with that achievable in other regions of the spectrum. Firstly, absorption spectroscopy with incoherent sources in any region will exhibit far smaller sensitivities than that obtained above because of the lack of brilliance of the source. Thus we can restrict our considerations to absorption spectroscopy with coherent sources. Secondly, many coherent sources are very noisy as the result of somewhat extraneous sources of noise such as vibration or plasma noise. Ion laser pumped cw dye lasers are such noisy sources. Because this excess laser noise is not intrinsic to the visible, varies widely in similar sources, and is difficult to estimate, we choose to ignore it in our calculations, only noting the case in which it is present. Thirdly, for absorption spectroscopy inside the laser cavity dP/dG is not known so that reliable estimates of the minimum detectable peak absorption coefficient are not available. The procedure adopted to make an estimate of the minimum detectable absorption coefficient is to scale the well established values for the microwave and FIR LMR by the frequency dependence of maser noise. All that remains then is to introduce the frequency dependence of the absorption coefficient (Eq. 10) and the dependence of the transition moment on whether a rotational, vibrational, or electronic transition is being considered. The resulting estimates of sensitivity are given in Table 2. The reasons for the rather notable success of FIR LMR in detecting transient species is quite evident from the table; it is probably the most sensitive absorption technique available! It is exceeded only by laser induced fluorescence, for which a concentration of 10^4 OH molecules/cm^3 can be probably detected.

V. ASSIGNING A SIMPLE LMR SPECTRUM

A simple linear Zeeman theory will be used to indicate the general methods of assigning a spectrum of CH. In the next section, we will develop a more general Zeeman theory used in the final analyses of LMR spectra.

Table 2. Comparison of Estimated Sensitivity of Various Absorption Spectroscopy Techniques for a Typical Small Molecule

Technique	ν (THz)	Estimated γ_o(min) (cm^{-1})	Estimated μ_{ij} (debye)	N(min) (cm^{-3})[a]
Microwave	.03	3×10^{-10}[b]	0.6[c]	3×10^{10}
FIR LMR	1.5	3×10^{-10}	0.5[d]	5×10^{7}
Mid-IR LMR	30	6×10^{-10}[e]	0.03	3×10^{8}
Visible cw Dye Laser	500	30×10^{-10}[f]	0.5[g]	7×10^{6}

[a] *Assumed line broadening parameter 10 MHz/Torr, total pressure = 1 Torr, T = 300 K and MW = 30 AMU.*

[b] *Although higher sensitivities are often reported, the pathlength is necessarily short for free radical systems.*

[c] *Assuming J = 1 ← 0 transition. For light molecules, low frequency transitions usually have small line strengths.*

[d] *Assuming μ_α = 1 debye, an R-branch transition and the strongest M component.*

[e] *Assuming sensitivity scales as the square root of quantum noise. The actual sensitivity depends on the properties of the mid-IR laser.*

[f] *Again assuming scaling as the square root of the quantum noise. This is a very generous estimate for a cw dye laser which is very noisy.*

Even using special techniques to defeat source noise, such as polarization spectroscopy, it is unlikely that this sensitivity will be approached.

[g] *Assuming an electronic transition moment of 1 debye, a Franck-Condon factor of 0.1 and a line strength of 15.*

To a first approximation the Zeeman energy, E_z, is

$$E_z = \mu_B g_J M_J B, \tag{11}$$

where μ_B is the Bohr magneton, g_J is the g factor of the level, M_J is the projection of J on B, and B is the magnetic flux density. LMR absorptions occur between levels of different J, and the absorption occurs when the levels are tuned an amount ΔE equal to the difference in energy between the laser and the rotational transition.

By subtracting the Zeeman energy of the lower level, E''_J, from the upper, E'_J, we get

$$\Delta E = \mu_B B(g'_J M'_J - g''_J M''_J). \tag{12}$$

For π transitions, M" = M', and the Zeeman tuning is

$$\Delta E = \mu_B B M''_J (g'_J - g''_J). \tag{13}$$

ΔE may be either positive or negative, and depending on the sign of $g'_J - g''_J$, either the positive or the negative values of M''_J may satisfy this equation. In either case the number of lines usually expected is $\frac{2J+1}{2}$. Solving for 1/B, we obtain

$$\frac{1}{B} = \frac{\mu_B(g'_J - g''_J)}{\Delta E} M''_J. \tag{14}$$

One would expect a series of LMR transitions to fall on a straight line with the 1/B intercept being either 0 or 1/2, depending on whether J is integer or half integer. Thus, to identify the M values belonging to the same set of lines, one need only plot 1/B vs a running number. In this way, the M''_J assignments can be made (providing the Zeeman effect is linear). For σ transitions, $M'_J = M''_J \pm 1$; therefore,

$$\Delta E = \mu_B B (\{g'_J - g''_J\} M''_J \pm g'_J), \tag{15}$$

and similarly,

$$\frac{1}{B} = \frac{\mu_B}{\Delta E} (\{g'_J - g''_J\} M''_J \pm g'_J). \tag{16}$$

Here, a plot of $\frac{1}{B}$ vs running number should produce a straight line of the same slope as the corresponding π series (i.e., the series with the same ΔE and $(g'_J - g''_J)$), but with different intercept depending on the value of g'_J. The number of lines expected depends on the value of g'_J compared with $\{g'_J - g''_J\} M''_J$, and often is the maximum number, 2J+1.

For many spectra, there is another technique for distinguishing between series of lines (lines differing only in M):

a "laser pulling experiment" is performed, i.e., $\Delta\nu/\Delta B$ is measured. The FIR laser is tuned to the high frequency side of its gain curve (typically $\Delta\nu \approx +2$ MHz), and the shift, ΔB, in line center is measured. For a linear Zeeman effect, the same series of lines (differing only in M) "pull" in the same direction, i.e., ΔB has the same sign.

We will now apply this to the CH spectrum shown in Fig. 3 and listed in Table 3. 1/B is plotted vs running number in

TABLE 3. Laser Magnetic Resonance Data for CH

Polarization	Line Center[a] (T)	Line Width[b] (G)	Relative Signal Amplitude
π	0.4258	47	9.3
	0.6628	62	13.0
	0.8242	58	9.6
	1.3221	93	8.7
	1.7147	140	4.3
σ	0.2316	21	1.0
	0.2924	29	3.3
	0.3968	36	5.2
	0.4116	33	1.0
	0.5275	33	2.4
	0.6171	48	5.3
	0.7377	47	3.8
	1.2694	83	3.9
	1.4173	113	3.7

[a] *Estimated uncertainties are ±5 G for lines below 10 kG and ±10 G for lines above 10 kG (1 T = 10 kG).*

[b] *Measured between peaks of the derivative line shape. Some of the narrower lines may be somewhat modulation broadened. These field widths are consistent with a frequency width of 21.5 MHz.*

[c] *Oscillator Frequency: 2527.953 ± 0.001 GHz.*

Fig. 8 for both π and σ lines. The predicted transition is J = 7/2 ← 5/2 and two lambda doublets are expected. (In this case, "pulling experiments" were not done, but would have been very useful since one lambda doublet series would have pulled positive and the other negative). Two separate σ series which appear quite linear are indicated by a_σ and b_σ. The two π series which exhibit slopes most similar to the corresponding σ slopes are shown by a_π and b_π. These possess slopes slightly

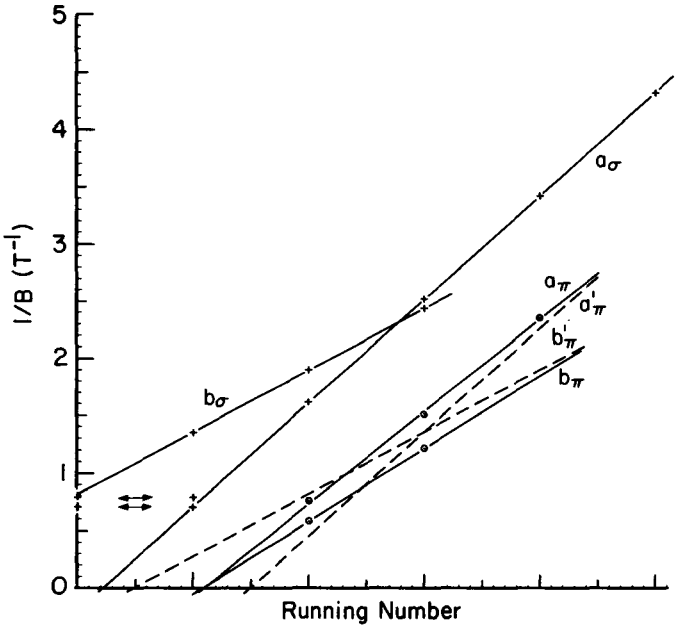

Fig. 8. Plot of 1/B versus running number for CH spectrum of Fig. 3.

different from those of a_σ and b_σ respectively, and do not have half integer intercepts. This is due to the non-linear effects. The slopes at low magnetic fields are the most linear and π slopes a'_π and b'_π are drawn through the most appropriate half integer points with the appropriate slope of either a_σ or b_σ. The divergence is quite obvious; however, a correct assignment of M''_J can be made from these plots and the spectrum was assigned as is shown in Fig. 9. The complete detailed analysis is given in Ref. 8. A wide variety of spectra have been observed from one extreme to the other - some nicely linear, as in $^1\Delta$ O_2, and some still not assignable such as in CH_2. In any case a complete and accurate fit to the precision attainable with LMR (about $\pm$ 1 MHz on the laser and $\pm$ 0.5 x 10^{-4} T on the magnetic field) requires the considerations indicated in the next section.

VI. THEORETICAL CONSIDERATIONS, MAINLY OF THE ZEEMAN INTERACTION

A far infrared LMR spectrum contains information about

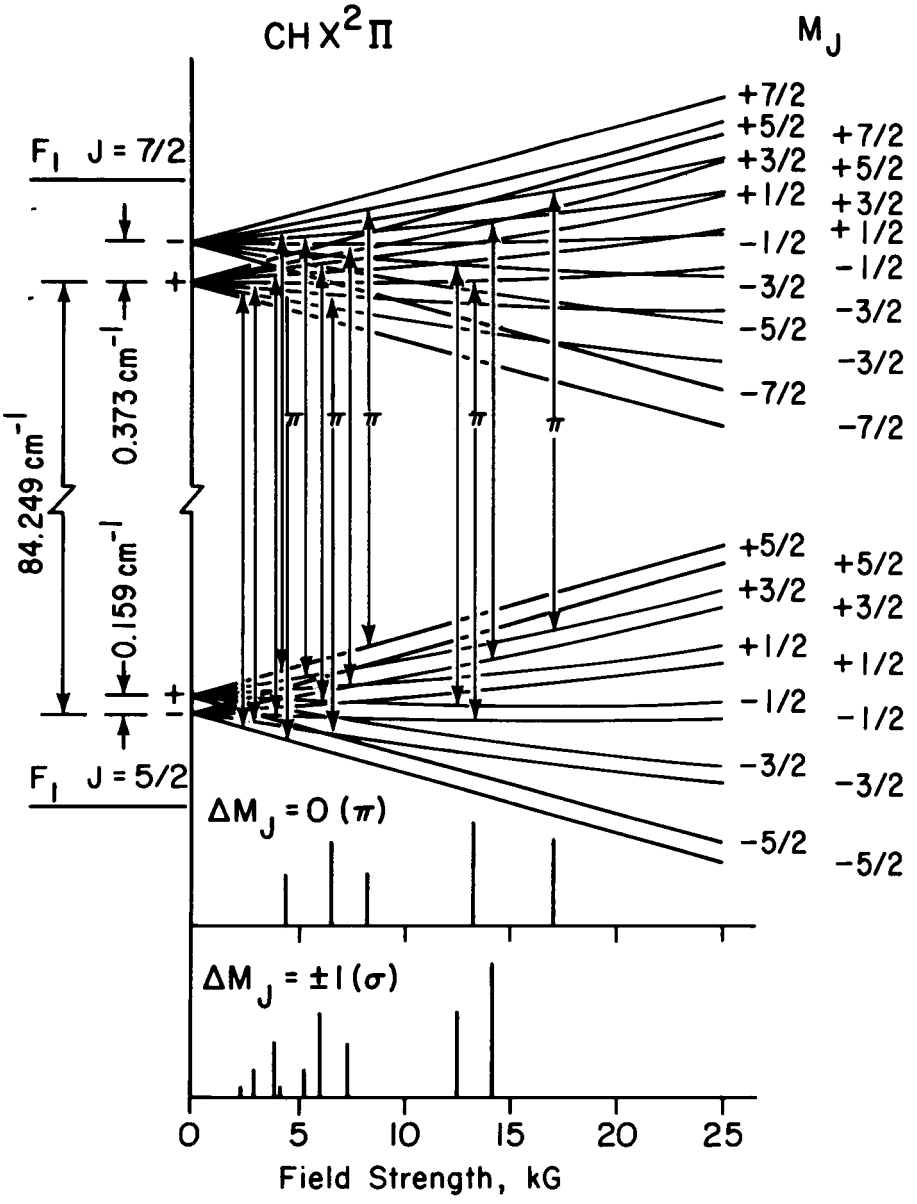

Fig. 9. CH Zeeman energy levels for J = 5/2 and J = 7/2 levels between 0 and 25 kG. The 118.6 μm observed transitions are identified for π-type polarization others are σ.

several distinct types of molecular interactions. There are zero-field contributions from (i) the rotational energy, (ii) electron spin fine structure, and (iii) the nuclear hyperfine structure. These terms account for almost all of the transition frequency and are, by and large, well documented in the literature. The zero-field Hamiltonian for diatomic molecules is covered in references (60) to (63) for example, while that for polyatomic molecules is given in references (64) and (65). In this section, we concentrate instead on the Zeeman effect, that is, the interaction between a molecule and an external magnetic field. Although comparatively small in magnitude, this interaction lies at the very heart of LMR spectroscopy by providing the frequency tuning which is essential to the experiment. In consequence, a proper understanding of the Zeeman effect is vital to the conception, execution, analysis and interpretation of an LMR experiment. Our treatment covers both diatomic and polyatomic (non-linear) molecules.

The classical expression for the energy of interaction between a magnetic dipole moment $\underline{m}$ and an applied flux density $\underline{B}$ is simply

$$\text{Zeeman energy} = -\underline{m} \cdot \underline{B}. \tag{17}$$

The magnetic moment $\underline{m}$ of a molecule arises from the motion of the charged particles of which it is constituted. The Zeeman Hamiltonian is obtained from equation (17) by making the appropriate quantum mechanical replacements. There are four distinct contributions, two from the "unpaired" electrons and two from the nuclei (see Table 4).

The operator expressions given in Table 4 are appropriate to a diatomic molecule but they apply equally well to a polyatomic molecule with the exception of the rotational magnetic moment. In the latter case, the scalar rotational g-factor must be replaced by a 2nd rank tensor to take account of the anisotropic distribution of nuclear charge:

$$m_\alpha = \mu_B \sum_\beta (g_r^N)_{\alpha\beta} R_\beta \tag{18}$$

where α,β stand for x, y or z. It should be noted from Table 4 that the electrons make a negative contribution to $\underline{m}$ while the nuclei (usually) make a positive contribution; this is simply a reflection of the sign of the charge on the particle concerned. While the electronic contributions to the magnetic moment predominate over those from the nuclei, they are present only if the molecule is in an open shell state; the nuclear contributions exist for any molecule. Perhaps the most important aspect of Table 4 is that, to a good

TABLE 4. First Order Contributions to the Magnetic Dipole Moment, $\underline{m}$

Origin	Operator	Magnitude
electron spin	$-g_S \mu_B \underline{S}$	$g_S = 2.0023$
electron orbital angular momentum	$-g_L \mu_B \underline{L}$	$g_L = 1.0000$
rotational angular momentum	$g_r^N \mu_B \underline{R}$	$g_r^N \sim 10^{-4}$
nuclear spin	$g_N \mu_N \underline{I}$	$g_N \sim 1$

μ_B is the Bohr magneton (1.3996 MHz/gauss) and μ_N is the nuclear magneton ($\mu_N = 5.45 \times 10^{-4} \mu_B$). $\underline{S}$, $\underline{L}$, $\underline{R}$ and $\underline{I}$ are the total electron spin, electron orbital, nuclear rotation and nuclear spin angular momenta, respectively.

approximation, the magnitudes of the various contributions to $\underline{m}$ depend simply on the particles concerned. A reliable prediction of the magnetic moment of a molecule in a particular state can therefore be made with some confidence; this is in marked contrast to the calculation of the electrical dipole moment, $\underline{\mu}$.

The Effective Hamiltonian

In principle, the energy levels of a molecule in a magnetic field can be calculated to any desired precision from the Hamiltonian derived from Eqn. (17). In practice, however, this is a huge task because the operator has off-diagonal matrix elements connecting not only different rotational states but also different vibrational and electronic states. A number of methods of averaging over the vibrational and electronic wavefunctions have been developed. We use the effective Hamiltonian approach in which the effects of the off-diagonal matrix elements are projected onto the vibronic state of interest by use of perturbation theory.[66,67] This procedure modifies the coefficients of the terms in the Hamiltonian in a well-defined way. It has the advantage of separating the two stages of spectrum analysis, namely (i) the fit of the experimental data by varying the coefficients or parameters in

the Hamiltonian, and (ii) the interpretation of the parameters in terms of electronic structure.

Some idea of how the effective Hamiltonian is constructed can be obtained by a study of the second order electronic terms. The second order contribution to the energy from a perturbation operator V to the zeroth order Hamiltonian H_o is given by the familiar expression

$$W^{(2)} = \sum_{n\neq o} (E_o - E_n)^{-1} \langle o|V|n\rangle\langle n|V|o\rangle. \tag{19}$$

Consider the cross term arising from two parts of the perturbation V, the spin-orbit coupling H_{so} which can be written phenomenologically as

$$H_{so} = \zeta \underline{L} \cdot \underline{S} \tag{20}$$

and the orbital Zeeman interaction

$$H_Z = g_L \mu_B \underline{L} \cdot \underline{B}. \tag{21}$$

The effect of these two operators when substituted in Eq. (19) is to produce the anisotropic corrections to the electron spin g-factor. This is shown schematically below for a diatomic molecule.

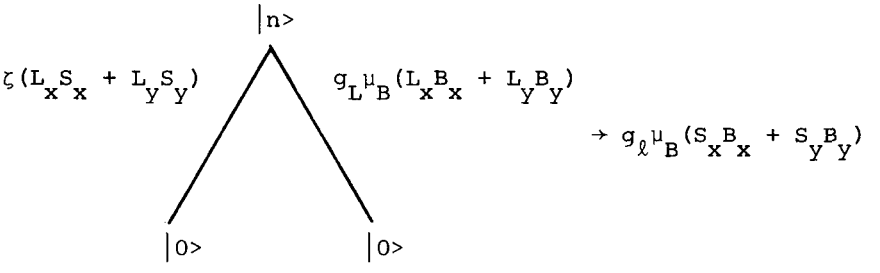

The resultant term in the effective Hamiltonian is shown on the right; the matrix elements and energy denominators in the perturbation expression have been absorbed into the parameter g_ℓ. Once again, the lower symmetry associated with a polyatomic molecule can be accommodated by the use of a tensor $\underline{g}_\ell$ in the place of the scalar. There are a number of similar 2nd order contributions to the effective magnetic moment, all involving cross terms with part of the Zeeman Hamiltonian so as to produce an operator linear in the flux density, $\underline{B}$.[68] They are itemized below. Contributions which are quadratic in $\underline{B}$ are also generated at this stage of the calculation, for example, by substitution of Eqn. (21) only in Eqn. (19).

These are the paramagnetic contributions to the molecular susceptibility, a subject which has been so beautifully treated by Van Vleck.[69] The effect of the molecular susceptibility on the Zeeman energy is much smaller than the precision of any LMR experiment performed to date, however, and it can be ignored for the moment.

The resultant effective Zeeman Hamiltonian for a diatomic molecule is[68]

$$\begin{aligned} H_Z = {} & g_S \mu_B \underline{S}\cdot\underline{B} + (g_L' + g_r)\mu_B \underline{L}\cdot\underline{B} - g_r \mu_B \underline{N}\cdot\underline{B} \\ & + g_\ell \mu_B (S_x B_x + S_y B_y) - g_N \mu_N \underline{I}\cdot\underline{B} \\ & - g_r^{e'} \mu_B (e^{-2i\phi} N_+ B_+ + e^{2i\phi} N_- B_-) \\ & + g_\ell' \mu_B (e^{-2i\phi} S_+ B_+ + e^{2i\phi} S_- B_-). \end{aligned} \tag{22}$$

In this Hamiltonian, g_S is the electron spin g-factor, g_L' is the electron orbital g-factor, corrected for non-adiabatic and other small effects, g_r is the rotational g-factor, N is the total mechanical angular momentum ($\underline{N} = \underline{L}+\underline{R}$), g_ℓ describes the anisotropic corrections to the electron g-factor (see above), and g_N is the nuclear spin g-factor. The remaining two parameters, g_ℓ' and $g_r^{e'}$, are only required for molecules in $^1\Pi$ states which show Λ-doubling; ϕ is the electron orbital azimuthal angle and N_- stands for $(N_x - iN_y)$, etc. Lower case letters x, y and z are used to indicate that the components are referred to a molecule-fixed axis system. A number of small details such as relativistic corrections, have been glossed over in the present treatment. They are described more fully in references 60 and 68.

It can be seen from Eq. (22) that there are six determinable Zeeman parameters at the present level of approximation (the nuclear spin g factor can be regarded as known from NMR studies since chemical shift effects are much too small to be detected by LMR). One aim of the experiment should be to provide sufficient data to determine all six of the parameters. The interpretation of these parameters in terms of electronic structure can then be effected by use of the expressions derived by perturbation theory.[68] It is worth noting that the rotational g-factor in Eq. (22) has two separate contributions,

$$g_r = g_r^N - g_r^e. \tag{23}$$

The first term is the nuclear contribution given in Table 4 and the second term is the electronic contribution which comes

from the second order perturbation treatment. As the nuclear framework of the molecule rotates, it drags the electrons around with it. The motion of the two types of particles together produces an approximate cancellation of their contributions to the magnetic moments, as implied by Eq. (23).

The corresponding effective Zeeman Hamiltonian for a non-linear molecule is [70]

$$H_Z = g_S \mu_B \underline{B} \cdot \underline{S} + g_L \mu_B \underline{L} \cdot \underline{B} + \mu_B \underline{B} \cdot \underline{g}_\ell \cdot \underline{S} - \mu_B \underline{B} \cdot \underline{g}_r \cdot \underline{S} - g_N \mu_N \underline{B} \cdot \underline{I} \quad (24)$$

The terms on the right hand side of Eq. (24) are analogous to those in Eq. (22). The scalar g-factors g_ℓ and g_r have been replaced by second rank tensorial quantities to take account of the lower symmetry of the molecule. There is one respect in which the Zeeman effect for polyatomic molecules is simpler than that for diatomics. Unless the molecule has a 3-fold or higher axis of symmetry (e.g., CH_3O), the orbital angular momentum is quenched and the effect of the second term in Eq. (24) vanishes. For the majority of problems, this term may therefore be omitted.

Most diatomic molecules studied so far by LMR are in $^2\Pi$ states. The "diagonal" part of the matrix representation of the effective Zeeman Hamiltonian for such molecules is given in Table 5 in a Hund's case (a), I-decoupled basis set.

Although other matrix elements, off-diagonal in J, M_J and M_I, are required to give a completely faithful representation of the Zeeman Hamiltonian, the essential features are contained in the matrix of Table 5. For example, since $g_L' \simeq 0.5\ g_S$, the magnetic moment of a molecule in the levels of the $^2\Pi_{1/2}$ component is very small; also the Zeeman effect in the $^2\Pi_{3/2}$ component decreases rapidly with J because of the $[J(J+1)]^{-1}$ dependence. The anisotropic correction to the spin g-factor, g_ℓ, enters only in the off-diagonal element and thus may be rather difficult to determine unless there is significant mixing of the two spin components by molecular rotation. The Zeeman effect for a molecule in a $^2\Pi$ state is usually close to linear over the whole available range of laboratory fields. This is because there is a first order splitting of the spin components by spin-orbit coupling which is much greater than the off-diagonal element of the matrix in Table 5.

The matrix representation of H_Z in Eq. (24) in a Hund's case (b) basis set for a polyatomic molecule in a ^2A state is given in Table 6; only the matrix elements diagonal in N are included. The dominant term in the matrix is that involving g_S. It is interesting to note that it has exactly the same form in the two spin components but the opposite sign.

TABLE 5. Diagonal Matrix Elements of the Zeeman Hamiltonian for a $^2\Pi$ State

$\lvert \pm; J\frac{3}{2} M_J M_I \rangle^a$	$\lvert \pm; J\frac{1}{2} M_J M_I \rangle^a$
$\mu_B B_o M_J \{3(g'_L + \frac{1}{2} g_S) -$	$\mu_B B_o M_J \{(g_S + g_\ell + g_r)$
$g_r [2(J+\frac{1}{2})^2 - 5]\}/[2J(J+1)]$	$\mp g_r^{e'} (J+\frac{1}{2})\}[(J-\frac{1}{2})$
$- g_N \mu_N B_o M_I$	$(J+\frac{3}{2})]^{1/2}/[2J(J+1)]$
	$\mu_B B_o M_J \{(g'_L - \frac{1}{2} g_S)$
	$-g_r [2(J+\frac{1}{2})^2 - 1]$
	$\pm (g'_\ell - g_r^{e'})(J+\frac{1}{2})\}/$
	$[2J(J+1)]$
	$- g_N \mu_N B_o M_I$

[a] *The upper and lower sign choices refer to e and f levels, respectively. The third quantum number in the kets is Ω, the projection of J on the internuclear axis.*

The rotational Zeeman effect, on the other hand, contributes to the energies of both F_1 and F_2 components with the same sense; it becomes more important with increasing N. There is no first order spin-orbit coupling for this type of molecule. The F_1 and F_2 components are separated by second order effects, which manifest themselves as spin-rotation coupling. This splitting is quite small (~1 cm^{-1}) for most of the molecules studied and the flux densities required for the off-diagonal element in the matrix of Table 6 to become comparable in magnitude are only a few tenths of a Tesla. In consequence the Zeeman effect is usually markedly non-linear, reflecting the progressive uncoupling of the electron spin from the molecular framework (the Paschen-Back effect). This behavior can be seen in Fig. 10. At very low fields, the splitting is linear in M_J because $\underline{S}$ is well-coupled to $\underline{N}$; at high fields, the Zeeman effect is linear in M_S because here $\underline{S}$ is decoupled.

TABLE 6. Diagonal Matrix Elements of H_Z for a Molecule in a ^2A State [a]

$\lvert NKF_1M_JM_I\rangle$	$\lvert NKF_2M_JM_I\rangle$
$\frac{\mu_B B_o M_J}{(2N+1)} \{g_S + \sqrt{6}(g_\ell)_{20}[3K^2-N(N+1)]$	$-\frac{\mu_B B_o[(N+\frac{1}{2})^2 - M_J^2]\frac{1}{2}}{(2N+1)} \{g_S - \sqrt{6}(g_\ell)_{20}$
$/[3(N+1)(2N+3)] \pm (g_\ell)_{22} N/(2N+3)$	$[3K^2-N(N+1)]/[12N(N+1)] \mp \frac{1}{4}(g_\ell)_{22}$
$+\frac{2}{3}\sqrt{3}(g_r)_{00}N - \sqrt{6}(g_r)_{20}[3K^2-N(N+1)]$	$-\frac{1}{3}\sqrt{3}(g_r)_{00} + \sqrt{6}(g_r)_{20}[3K^2-N(N+1)]$
$/[3(N+1)] \mp (g_r)_{22}N\} - g_N\mu_N B_o M_I$	$/[6N(N+1)] \pm \frac{1}{2}(g_r)_{22}\}$
	$-\frac{\mu_B B_o M_J}{(2N+1)} \{g_S + \sqrt{6}(g_\ell)_{20}[3K^2-N(N+1)]$
	$/[3N(2N-1)] \pm (g_\ell)_{22}(N+1)/(2N-1)$
	$-\frac{2}{3}\sqrt{3}(g_r)_{00}(N+1) + \sqrt{6}(g_r)_{20}[3K^2-N(N+1)]$
	$/(3N) \pm (g_r)_{22}(N+1)\} - g_N\mu_N B_o M_I$

[a] See following page.

[a] *The states labeled F_1 and F_2 are the two spin components of a given rotational level N of a molecule in a doublet state. The parameter combinations are related to those of Eq. (24) by*

$$\sqrt{3}(g_r)_{00} = -(g_r^{xx} + g_r^{yy} + g_r^{zz})$$

$$\sqrt{6}(g_r)_{20} = 2g_r^{zz} - g_r^{xx} - g_r^{yy}$$

$$(g_r)_{22} = 1/2(g_r^{xx} - g_r^{yy}), \text{ with similar}$$

expressions for $(g_\ell)_{kq}$. The terms preceded by a $\pm$ sign choice are included for levels with K = 1 only; the upper and lower sign choices refer to the upper (b) and lower (a) K doublets, respectively.

Estimation of Zeeman Parameters

There are many parameters in the Zeeman Hamiltonians given above. At the start of the analysis of a new LMR spectrum, none of the values of these parameters are known and the prediction of Zeeman splittings might seem a daunting task. Fortunately, this is not so for two reasons. First, the electronic contributions (g_L and g_S) to the magnetic moment are predominant and estimates which are reliable to a few parts in 10^3 can be made simply by setting $g_L = 1.000$ and $g_S = 2.002$. In other words, the gross effects are completely predictable. Secondly, reliable formulae for estimating some of the non-adiabatic corrections to the magnetic moment are available. The best known is Curl's relationship[71,72] which allows the anisotropic corrections to the spin g-factor to be estimated from spin-rotation constants. The relationship is

$$g_\ell = -\gamma/2B \tag{25}$$

for a diatomic molecule and

$$g_\ell^{\alpha\alpha} = -\varepsilon_{\alpha\alpha}/2B_{\alpha\alpha} \tag{26}$$

for a polyatomic molecule; γ and $\varepsilon_{\alpha\alpha}$ are the spin-rotation constants, B and $B_{\alpha\alpha}$ are the rotational constants. The formula has been tested for many molecules and has been found reliable, particularly if only first or second row elements are involved. Several relationships between the g-factors of

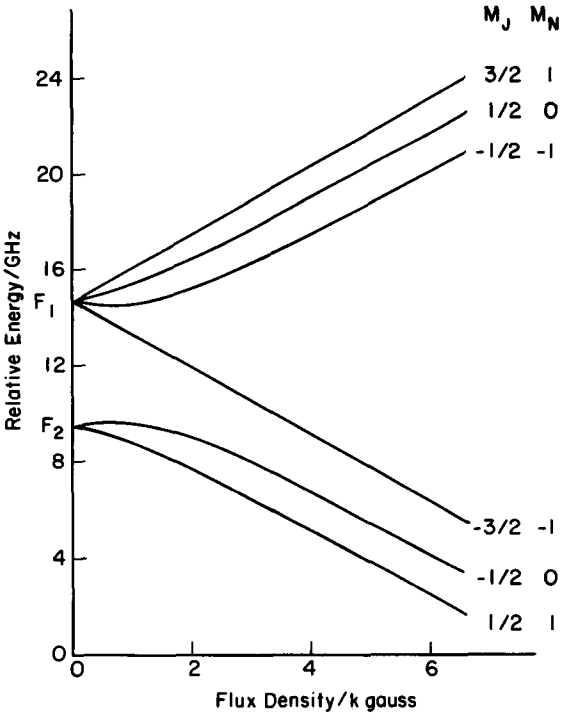

Fig. 10. Spin uncoupling in the levels of a polyatomic molecule by application of an external magnetic field (the Paschen-Back effect). At very low fields, the spin is coupled to molecular rotation and the Zeeman splitting is linear in M_J. At high fields, the spin is oriented with respect to the magnetic field direction and the Zeeman splitting is linear in M_S. The lower set of levels correspond to $M_S = -1/2$ and the upper levels to $M_S = 1/2$. Note that $M_J = M_N + M_S$.

Eq. (23) can be established from perturbation theory on making some assumptions about the electronic states; details are given in ref. 68. There are also some useful relationships analogous to Eq. (25) which involve the Λ-type doubling parameters:

$$g_\ell' \simeq p/2B \tag{27}$$

and

$$g_r^{e'} \simeq -q/B. \tag{28}$$

Finally, there is a relationship for estimating the electronic contributions to the rotational g-factors:[73]

$$g_r^{\alpha\alpha} \simeq -|\varepsilon_{\alpha\alpha}|/\zeta, \tag{29}$$

where ζ is an appropriately weighted (atomic) spin-orbit coupling parameter.

The use of these various formulae make the prediction of Zeeman effect a fairly straightforward procedure. Once the spectrum has been fitted, of course, the perturbation formulae can be used in reverse to reach conclusions about the electronic structure. So far, a "complete" determination of Zeeman parameters has been achieved in only one case, the free radical OH in its $X^2\Pi$ state.[68] The results are reproduced in Table 7, along with theoretical values estimated from some of the formulae above and also from a simple theoretical model (pure precession) appropriate for OH. The formulae can be seen to be very reliable in this case.

TABLE 7. Zeeman Parameters for OH in the $X^2\Pi$ State

Parameter	*Experimental*[a]	*Estimated*[b]	*Calculated*[c]
g_L'	*1.00107(15)*	.....	*1.00093*
g_S	*2.00152(36)*	.....	*2.00206*
$10^3\, g_\ell$	*4.00(56)*	*3.20*	*4.29*
$10^3\, g_r$	*-0.633(19)*	.....	*-0.55*
$10^3\, g_\ell'$	*6.386(30)*	*6.347*	*8.58*
$10^3\, g_r^{e'}$	*2.0446(23)*	*2.087*	*2.19*

[a] *Values taken from Ref. 68. The numbers in parentheses represent one standard deviation, in units of the last quoted decimal place.*

[b] *Values calculated from Eqs. (25), (27) and (28) of this paper.*

[c] *Values calculated assuming that the $X^2\Pi$ and $A^2\Sigma^+$ state are in pure precession. The relativistic correction was taken as 1.30×10^{-4}.*

Concluding Remarks

Some of the useful characteristics of the Zeeman interaction have already been mentioned, namely its predictability and use as a source of information on electronic structure.

In addition, we note that parity is not destroyed by a magnetic field which is advantageous in calculations of the Zeeman effect. Again the Zeeman patterns in LMR spectroscopy are highly personal signatures of the transitions involved. While they can at times be baffling, their interpretation is usually unambiguous. Although not fully established, another desirable characteristic of the Zeeman parameters is emerging from recent LMR studies, that is, their weak dependence on vibrational coordinates. This is not very surprising since we have seen that they are mainly electronic in origin. It means that large centrifugal distortion or vibrational dependencies of the Zeeman parameters are not to be expected.

It remains only to question mildly the reliability of the Zeeman Hamiltonian presented here. It must be remembered that it is good to second order in perturbation theory only. If large spin-orbit effects are involved (heavy elements), third and higher order contributions can be significant.[74] These contributions not only modify existing second order parameters but also introduce terms of completely different operator form.[75] Another difficulty in the interpretation of Zeeman data results from the indeterminacies in the molecular Hamiltonian. These have been investigated in some detail for diatomic molecules;[63] they can be eliminated by the application of appropriate similarity transformations. The transformations also affect the Zeeman terms in the Hamiltonian. For example, if the data for a molecule in a $^2\Pi$ state are fitted to a Hamiltonian with A_D constrained to zero, two of the g-factors become effective parameters given by:

$$\tilde{g}_L' = g_L' + (1/4)\, g_S A_D/B \tag{30}$$

$$\tilde{g}_\ell = g_\ell - (1/2)\, g_L' A_D/B. \tag{31}$$

In addition, two other terms of completely different operator form are generated in the Hamiltonian by the reduction processes.[76] Such effects, which are very small, have not yet been detected in an experimental study.

VII. CONCLUSION

Laser Magnetic Resonance, with its high sensitivity and high resolution, has produced detailed spectroscopic information on a number of interesting transient species which have eluded detection by other high resolution techniques. These

same qualities of LMR should make it possible to detect certain astrophysically important radicals for which only theoretical (ab initio) estimates of parameters are available. The recent detection of LMR spectra from short-lived metastable electronic states and a molecular ion demonstrates that these difficult classes of radicals are now amenable to study by this method. The continued discovery of additional FIR laser lines increases the probability of the near coincidences needed for LMR studies. Many exciting new results are likely to proceed from this area in the next few years.

REFERENCES

1. Carrington, A., "Microwave Spectroscopy of Free Radicals", Academic Press, New York (1974).
2. Knight, D. J. E., National Physical Laboratory, Teddington, Middx. U.K.; Report #QU 45, March, 1979.
3. Evenson, K. M., Broida, H. P., Wells, J. S., Mahler, R. J., and Mizushima, M., *Phys. Rev. Lett. 21,* 1038 (1968).
4. Wells, J. S. and Evenson, K. M., *Rev. Sci. Inst. 41,* 227 (1970).
5. Evenson, K. M. and Wells, J. S., *IEEE J. Quantum Electron. QE-6,* 184 (1970).
6. Curl, Jr., R. F., Evenson, K. M., and Wells, J. S., *J. Chem. Phys. 56,* 5144 (1972).
7. Evenson, K. M., Wells, J. S., and Radford, H. E., *Phys. Rev. Lett. 25,* 199 (1970).
8. Evenson, K. M., Radford, H. E., and Moran, Jr., M. M., *Appl. Phys. Lett. 18,* 426 (1971).
9. Mizushima, M., Evenson, K. M., and Wells, J. S., *Phys. Rev. A 5,* 2276 (1972).
10. Evenson, K. M. and Mizushima, M., *Phys. Rev. A 6,* 2197 (1972).
11. Tomuta, L., Mizushima, M., Howard, C. J., and Evenson, K. M., *Phys. Rev. A 12,* 974 (1975).
12. Radford, H. E., Evenson, K. M., and Howard, C. J., *J. Chem. Phys. 60,* 3178 (1974).
13. Hougen, Jon T., *J. Mol. Spectrosc. 54,* 447 (1975).
14. Hougen, Jon T., Radford, H. E., Evenson, K. M., and Howard, C. J., *J. Mol. Spectrosc. 56,* 210 (1975).
15. Cook, J. M., Evenson, K. M., Howard, C. J., and Curl, Jr., R. F., *J. Chem. Phys. 64,* 1381 (1976).
16. Davies, P. B., Russell, D. K., Thrush, B. A., and Wayne, F. D., *J. Chem. Phys. 62,* 3739 (1975).

17. Davies, P. B., Russell, D. K., and Thrush, B. A., *Chem. Phys. Lett. 36,* 280 (1975).
18. Davies, P. B., Russell, D. K., and Thrush, B. A., *Chem. Phys. Lett. 37,* 43 (1976).
19. Howard, C. J. and Evenson, K. M., *J. Chem. Phys. 61,* 1943 (1974).
20. Howard, C. J. and Evenson, K. M., *J. Chem. Phys. 64,* 4303 (1976).
21. Howard, C. J. and Evenson, K. M., *J. Chem. Phys. 64,* 197 (1976).
22. Howard, C. J., *J. Chem. Phys. 65,* 4771 (1976).
23. Howard, C. J. and Evenson, K. M., *Geophys. Res. Lett. 4,* 437 (1977).
24. Crutzen, P. J. and Howard, C. J., *Pure Appl. Geophys. 116,* 497 (1978).
25. Howard, C. J., *J. Chem. Phys. 67,* 5258 (1977).
26. Thrush, B. A., Harris, G. W., and Burrows, J. P., *Nature, 267,* 233 (1977).
27. Hack, W., Preuss, A. W., and Wagner, H. Gg., *Ber. Bunsenges. Phys. Chem. 82,* 1167 (1978).
28. Hack, W., Preuss, A. W., Wagner, H. Gg., and Hoyermann, K., *Ber. Bunsenges. Phys. Chem. 83,* 212 (1979).
29. Stimpfle, R. M., Perry, R. A., and Howard, C. J., *J. Chem. Phys. 71,* 5183 (1979).
30. Howard, C. J., *J. Chem. Phys. 71,* 2352 (1979).
31. Zahniser, M. S. and Howard, C. J., in preparation.
32. Chang, T. Y. and Bridges, T. J., *Opt. Commun. 1,* 423 (1970).
33. Radford, H. E. and Litvak, M. M., *Chem. Phys. Lett. 34,* 561 (1975).
34. Wayne, F. D. and Radford, H. E., *Mol. Phys. 32,* 1407 (1976).
35. Davies, P. B., Russell, D. K., Thrush, B. A., and Radford, H. E., *Proc. R. Soc. Lond. A, 353,* 299 (1978).
36. Radford, H. E. and Russell, D. K., *J. Chem. Phys. 66,* 2223 (1977).
37. Evenson, K. M., Jennings, D. A., Petersen, F. R., Mucha, J. A., Jimenez, J. J., Charlton, R. M., and Howard, C. J., *IEEE J. Quantum Electron. QE-13,* 442 (1977).
38. Hougen, J. T., Mucha, J. A., Jennings, D. A., and Evenson, K. M., *J. Mol. Spectrosc. 72,* 463 (1978).
39. Mucha, J. A., Jennings, D. A., Evenson, K. M., and Hougen, J. T., *J. Mol. Spectrosc. 68,* 122 (1977).
40. Davies, P. B., Handy, B. J., Murray-Lloyd, E. K., and Smith, D. R., *J. Chem. Phys. 68,* 1135 (1978).
41. Davies, P. B., Handy, B. J., Murray-Lloyd, E. K., and Russell, D. K., *Mol. Phys. 36,* 1005 (1978).

42. Davies, P. B., Handy, B. J., Murray-Lloyd, E. K., and Russell, D. K., *J. Chem. Phys. 68,* 3377 (1978).
43. Mucha, J. A., Evenson, K. M., Jennings, D. A., Ellison, G. B., and Howard, C. J., *Chem. Phys. Lett. 66,* 244 (1979).
44. Evenson, K. M., Saykally, R. J., and Hougen, J. T., "Far-Infrared Laser Spectra of Methylene", 34th Symposium on Molecular Spectroscopy, Columbus, OH; June, 1979; Paper TF-5.
45. Saykally, R. J. and Evenson, K. M., "The Ethynyl Radical (CCH) Detected by Laser Magnetic Resonance", 33rd Symposium on Molecular Spectroscopy, Columbus, OH; June, 1978; Paper FB-8.
46. Tucker, K. D., Kutner, M. L., and Thaddeus, P., *Astrophys. J. 193,* L115 (1974).
47. Saykally, R. J. and Evenson, K. M., "The Far-Infrared Laser Magnetic Resonance Spectrum of CF", 34th Symposium on Molecular Spectroscopy, Columbus, OH; June, 1979; Paper TF-4.
48. Saykally, R. J. and Evenson, K. M., *Astrophys. J. 238,* L1 (1980).
49. Scalabrin, A., Mizushima, M., Saykally, R. J., Radford, H. E., and Evenson, K. M., "Laser Magnetic Resonance Spectrum of the $a^1\Delta_g$ state of O_2", in preparation.
50. Saykally, R. J. and Evenson, K. M., *J. Chem. Phys. 71,* 1564 (1979).
51. Dixon, T. A. and Woods, R. C., *Phys. Rev. Lett. 34,* 61 (1975).
52. Woods, R. C., Dixon, T. A., Saykally, R. J., and Szanto, P. G., *Phys. Rev. Lett. 35,* 1269 (1975).
53. Saykally, R. J., Dixon, T. A., Anderson, T. G., Szanto, P. G., and Woods, R. C., *Astrophys. J. 205,* L101 (1976).
54. Dixon, T. A. and Woods, R. C., *J. Chem. Phys. 67,* 3956 (1977).
55. Saykally, R. J., Szanto, P. G., Anderson, T. G., and Woods, R. C., *Astrophys. J. 204,* L143 (1976).
56. Saykally, R. J., "Microwave Spectroscopy of Transient Molecular Species in Glow Discharges", Ph.D. Thesis, University of Wisconsin (1977).
57. Saykally, R. J. and Evenson, K. M., "Far-Infrared Laser Magnetic Resonance Spectra of $a^3\Pi$ CO", 34th Symposium on Molecular Spectroscopy, Columbus, OH; June, 1979; Paper TF-6.
58. Saykally, R. J. and Evenson, K. M., *Phys. Rev. Lett. 43,* 515 (1979).
59. Kimble, H. J., *IEEE J. Quantum Electron. QE-16,* 455 (1980).

60. Carrington, A., Levy, D. H., and Miller, T. A., *Adv. Chem. Phys. 18,* 149 (1970).
61. Frosch, R. A. and Foley, H. M., *Phys. Rev. 88,* 1337 (1952).
62. Zare, R. N., Schmeltekopf, A. L., Harrop, W. J., and Albritton, D. L., *J. Mol. Spectrosc. 46,* 37 (1973).
63. Brown, J. M., Colbourn, E. A., Watson, J. K. G., and Wayne, F. D., *J. Mol. Spectrosc. 74,* 294 (1979).
64. Watson, J. K. G., "Vibrational Spectra and Structure" (J. R. Durig, ed.), Vol. 6, Elsevier, Amsterdam, 1977.
65. Brown, J. M. and Sears, T. J., *J. Mol. Spectrosc. 75,* 111 (1979).
66. Pryce, M. H. L., *Proc. Phys. Soc. A63,* 25 (1950).
67. Miller, T. A., *Mol. Phys. 16,* 105 (1969).
68. Brown, J. M., Kaise, M., Kerr, C. M. L., and Milton, D. J., *Mol. Phys. 36,* 553 (1978).
69. Van Vleck, J. H., "The Theory of Electric and Magnetic Susceptibilities", Oxford University Press, London (1932).
70. Bowater, I. C., Brown, J. M., and Carrington, A., *Proc. Roy. Soc. A333,* 265 (1973).
71. Curl, Jr., R. F., *Mol. Phys. 9,* 585 (1965).
72. Tinkham, M. and Strandberg, M. W. P., *Phys. Rev. 97,* 951 (1955).
73. Barnes, C. E., Brown, J. M., Carrington, A., Pinkstone, J., Sears, T. J., and Thistlethwaite, P. J., *J. Mol. Spectrosc. 72,* 86 (1978).
74. Miller, T. A., *J. Chem. Phys. 54,* 3156 (1971).
75. Brown, J. M., Carrington, A., and Sears, T. J., *Mol. Phys. 37,* 1837 (1979).
76. Brown, J. M., unpublished results.
77. Phillips, T. G., Huggins, P. J., Kuiper, T. B. H., and Miller, R. E., *Astrophys. J. 238,* L6 (1980).